Tampere University

Jorge Jiménez

COMPARISON OF MICROSTRUCTURES OBTAINED BY ISOTHERMAL HEAT TREATMENTS ON STEELS

Transmission Electron Microscopy Analysis

Faculty of Engineering and Natural Sciences
Master of Science Thesis
January 2020

ABSTRACT

Jorge Jiménez: Comparison of microstructures obtained by isothermal heat treatments on steels. Transmission Electron Microscopy Analysis.
Master of Science Thesis
Tampere University
Double Master's Degree in Materials Science and Engineering
January 2021

Steels are one of the most used materials in the world. Iron has been studied since it was used for the first time, and yet there are many questions unsolved. Bainite, a microstructure that is neither perlite nor martensite, is one of the most conspicuous examples. Although now there is indication that the transformation by which it is formed is displacive, it has been topic of discussion for decades.

In this work, the focus will be on the effect of the heat treatment on carbon distribution, including carbon compounds precipitation, and the accommodation of strain associated to the bainitic and martensitic transformations. In order to achieve this, we have compared the microstructures resulting from different isothermal heat treatments: quenching and tempering, and austempering, respectively.

A high-carbon, high-silicon steel (0.66C-1.45Si-1.35Mn-1.02Cr wt%) was selected and heat treated. Isothermal temperature treatments were 200ºC in both cases, quenching and tempering consisted of austenization at 900ºC, quenching to room temperature, and tempering at 200º; austempering consisted of a similar austenization, but partial quenching to 200ºC directly, avoiding complete cooling of the sample.

The characterization included X-Ray Diffraction and Transmission Electron Microscopy. XRD was used to determine lattice parameters, volume fraction of the phases and microstrain overall the sample. TEM, on the other hand, allowed characterization of the microstructure and phases at microscale.

Results showed higher carbon distribution ferrite in the martensitic samples than in the bainitic ones. In bainites, carbon can partition during the transformation, stabilize the austenite leading to higher volume fraction of this phase than in martensite microstructure. In addition, carbon precipitation is finer in bainite than in martensite. Findings included new evidence of carbon clustering of $Fe_{16}C_2$ in martensitic ferrite.

Keywords: Metallurgy; Isothermal treatments; Bainite; Martensite; Electron Microscopy

PREFACE

This document compiles the work I have done for the realization of this Master's Thesis in Materials Engineering during the 2018-2019 academic year, at the Tampere Universities (TAU), at the Faculty of Engineering and Natural Sciences.

I would like to show my gratitude for all the people that made it possible. I want to thank my parents and family because they have never lost confidence in me. Without their support I could have never got that far.

I want to thank my teachers, supervisors and instructors who guided me along this path. They helped me to reach my goals and advised me on every choice making I had to face.

I want to thank my partner, my friends and all people that shared this experience with me during these years, but especially those who were with me this last one. They have filled my time with good memories that I will always remember.

This concludes on of the most important chapters of my life.

Tampere, 20 October 2019

Jorge Jiménez

CONTENTS

LIST OF FIGURES AND TABLES

LIST OF SYMBOLS AND ABBREVIATIONS

Units

kg	kilogram	Mass
g	gram	Mass
m	meter	Length
µm	micron	Length
nm	nanometre	Length
K	Kelvin	Temperature
mol	mol	Chemical quantities
J	Joules	Energy
W	Watts	Power

Roman symbols

A_1	Eutectic temperature; Starting α-γ transformation
A_3	Temperature to which α-γ transformation is completed. (hypoeutectoid)
A_{CM}	Temperature to which α-γ transformation is completed. (hypereutectoid)
A_s	Temperature at which austenization starts during heating
A_f	Temperature at which austenization completes during heating
a, c	Lattice parameters: *a* for cubic lattices; *a* and *c* for tetragonal lattices
B_S	Highest temperature at which isothermal treatment produces bainite
M_S	Martensite transformation starting temperature
M_{50}	Temperature at which martensitic transformation is 50% completed
M_{90}	Temperature at which martensitic transformation is 90% completed
C_α	Carbon concentration in ferrite matrix
C_γ	Carbon concentration in austenite matrix
$C_{dislocation}$	Carbon concentration associated to dislocation defect
$C_{cluster}$	Carbon concentration in clusters
$C_{carbide}$	Carbon concentration in carbide (cementite)

Greek symbols

α	Proeutectoid ferrite
α_m	Primary ferrite
α_b	Bainitic ferrite
α’	Martensitic ferrite
γ	Austenite
γ_r	Retained austenite
δ	Delta ferrite
θ	Cementite (Fe_3C)
⊥	Dislocation

Acronyms and Abbreviations

TAU	Tampere University
UPM	Universidad Politécnica de Madrid

CSIC	Consejo Superior de Investigaciones Científicas (Superior Council of Scientific Investigations)
CENIM	Centro Nacional de Investigaciones Metalúrgicas (National Center for Metallurgical Research)
RT	Room temperature (~25ºC)
BC	Before Christ
AD	Anno Domini (After Christ)
BCC	Body Centred Cubic
BCT	Body Centred Tetragonal
FCC	Face Centred Cubic
CCT	Continuous Cooling Transformation diagrams
TTT	Temperature-Time-Transformation diagrams
APT	Atom Probe Tomography
XRD	X-Ray Diffraction
TEM	Transmission Electron Microscopy
TMC	Tampere Microscopy Center
STEM	Scanning Transmission Electron Microscopy
BF	Bright Field
DF	Dark Field
ED	Electron Diffraction
SAED	Selected Area Electron Diffraction
ZA	Zone Axis
EDX	Energy Dispersive X-ray spectroscopy
EELS	Electron Energy Loss Spectroscopy

1. INTRODUCTION

Steel can be defined as an alloy family constituted by iron with the addition of carbon. It is, by far, the most used metallic material in the world. One probable explanation is the wide availability as a natural resource, but even more important are the physical properties and complexity that make steel one of the most versatile materials. Steel cost effectiveness is related both to iron abundance and exceptional performance.

1.1 Iron and steel

Iron is the most abundant element in the Earth, being the main constituent of the planetary core [1]. In the outer crust, where we can reach it, it is the fourth most abundant element, being iron oxides the major contributor to this value [2].

Most common element of alloy for iron is carbon. Carbon atoms usually come from the processing of iron from its ore because most of these methods involve the use of coal or coke. Over the history of this metal, a vast number of combinations emerged, but steel is the most used iron base alloy.

Steel is by far the most used metallic material in the world, around 94% of metallic materials that are produced are iron-base products, 56% corresponds to raw steel, Figure 1. Its most important usage is in construction. Its abundance as a natural resource plays a very important role in its low price.

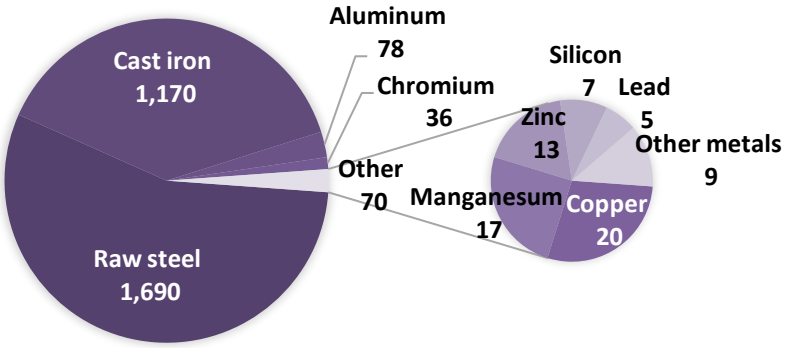

Figure 1. World production of materials from primary sources in 2017. Data in million metric tones [3].

Iron production from ore started around second millennium before Christ [4]. Nowadays, one of the main sources of raw material for steel production is scrap [5]. Steel is one of the most recycled materials in the world, around 86% of raw steel production feeds on recycling [6]. This circular model of economy not only reduces the waste that this industry generates; but also, the energy required to produce a ton of steel today is only 40% than was required 50 years ago [7].

The industry of iron and steel is constantly increasing. In 2004 global raw steel production reached for the first time the annual billion tonnes milestone. During the 2008 economic recession, steel production dropped in almost every country except in China. Since 2013 this country manufactures approximately half of the total production, Figure 2.

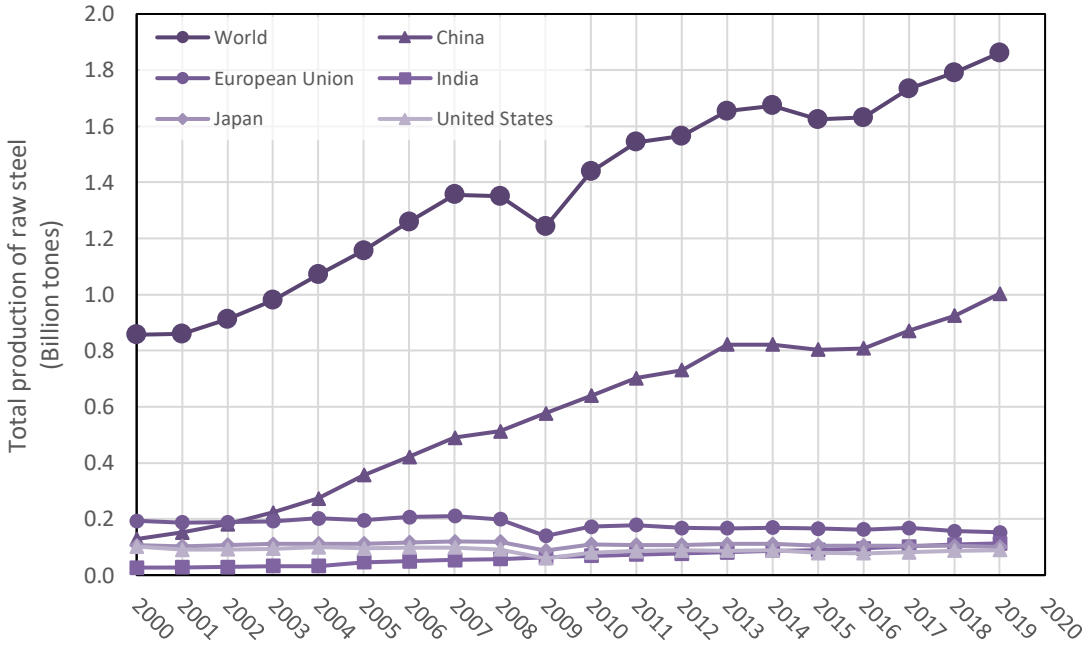

Figure 2. Total production of crude steel. Comparison between the global production of the five most important contributors, [8].

To sum up, steels and other iron-based materials come from very abundant natural resources, production is well industrialized and automatized, and recycling yields few to no degradation. This has allowed steel to be one of the most widely used materials in the world, and the most widely used metal in history. However, the most interesting aspects of steel research lie in its physical characteristics.

Iron is the twenty sixth element in the periodic table. It belongs to the group eight, first from transitions elements, and fourth period. Its standard atomic weight is 55.845(2) g/mol [9], a molar heat capacity of 25.10 J/(mol·K). Pure iron melting point is 1538ºC

(1811K) and thermal conductivity is 80.4 W/(m·K). Around room temperature, thermal expansion is 11.8 μm/(m·K) and density is 7,874 kg/m^3. It is also a ferromagnetic metal; its Curie temperature is at 770ºC.

Its atoms form a body centred cubic crystalline structure (BCC) known as ferrite, except in the temperature range from 912ºC to 1394ºC, where it suffers an allotropic transformation and arranges in face centred cubic lattice (FCC) known as austenite; Figure 3. Ferrite formed at lower temperatures than austenite is referred by the greek letter alpha, α; and delta, δ, when it is formed above. Austenite is referred by the letter gamma, γ [10].

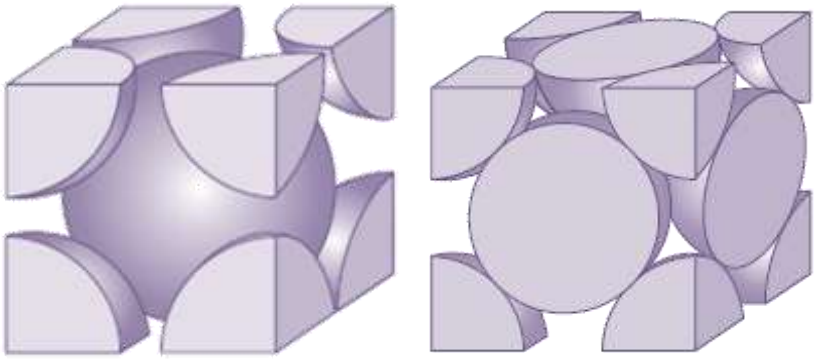

Figure 3. Body centred cubic and face centred cubic lattices unit cells on left and right respectively [10]. *BCC unit cell contains of 2 atoms, eight eighths on the corners and one in the center, while FCC unit cell contains 4 atoms, eight eighths in the corners and six halfs in the center of each face.*

The allotropic transformation α-γ makes steel one of the most versatile materials. In materials science, it is well known that properties depend on the structure of the material at atomic scale, and in this case, BCC and FCC lattice correspond to different behaviours. Furthermore, materials properties are strongly related to microstructural features as grain size, morphology, and orientation texture, among others. In ferritic steels, austenite transformation can be used to obtain specific microstructures and to reach exceptional properties.

1.2 Heat treatments

Any process which, through the application of a thermal cycle that makes possible to modify the microstructure, composition and, ultimately, the physical and mechanical properties of the materials is known as heat treatment. The influence of temperature cycles on mechanical properties is known since early metallurgy; first quenching date from fourth-century BC [11].

Heat treatments can produce many different effects in metals microstructure, depending on the composition and temperatures it goes through. We can classify almost every alloy of every metal depending on the heat treatments that can be applied.

These treatments are designed using the thermal stability of the material. Phase diagrams of materials represents the microstructure (phase or phases, and proportion of each) that appears in an alloy as a function of composition and temperature in equilibrium. This equilibrium is obtained when the material has had enough time and energy to stabilize in those conditions.

Figure 4 shows the phase diagram of iron and carbon alloy. Steel is defined as the family or families of iron alloy with a carbon concentration up to 2.14% in weight. In the diagram we can determine that steels are restricted by the maximum solubility of carbon in austenite. That means that, theoretically, in every steel it is possible to obtain a fully austenite structure at some temperature. From 2.14% the alloy is known as cast iron, since the melting point drops drastically, to 6.67% which corresponds to the composition of iron carbide, Fe_3C.

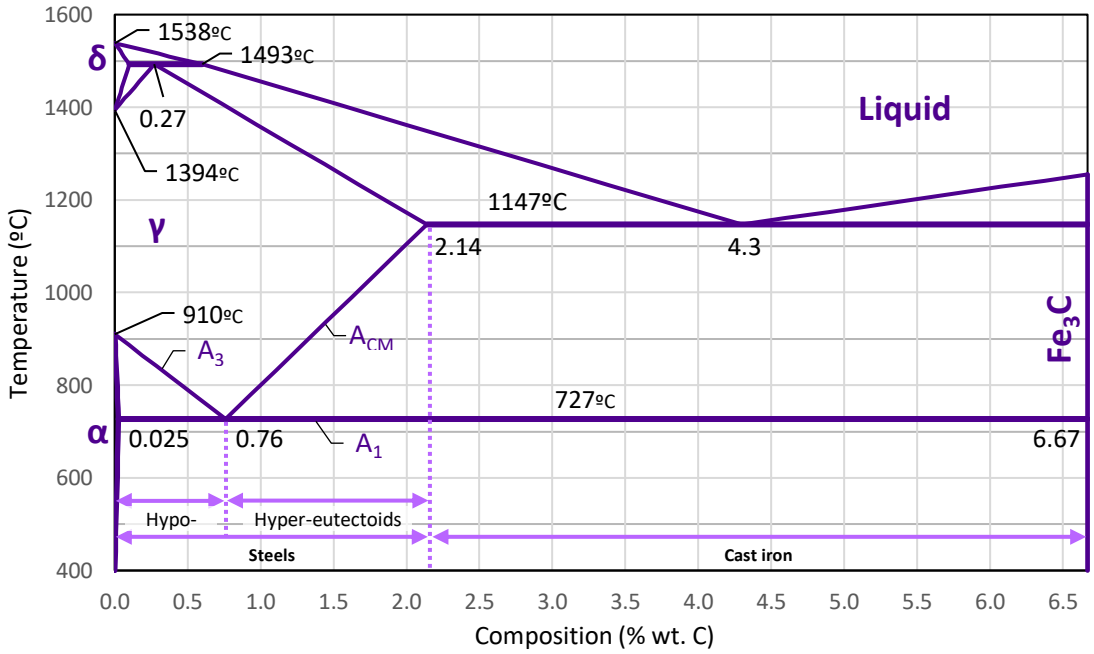

Figure 4. Iron-Carbon (Cementite) phase diagram [10].

In steels, the allotropic transformation from α to γ is eutectoid. That means that there is a minimum temperature at which a certain carbon concentration is fully soluble.

This concentration is around 0.76% wt. of carbon. Steels are classified in hypoeutectoids below this concentration and hypereutectoids above. Hypoeutectoid steels have the

characteristic that when cooled down from austenite, they first start forming ferrite while austenite increases its carbon content, following A_3 until reaches 727ºC, when remainder γ carbon concentration is 0.76 and austenite decomposes into both α and cementite in lamellar mixture, known as pearlite. On the other hand, hypereutectoid steels follow a similar evolution, but first phase precipitating is cementite, leaving a final microstructure of cementite and pearlite [12].

Furthermore, the phase diagram shown above represents the equilibrium state for Fe-C alloy, but alloying elements shift those phase limits values, both temperature and composition. Alloying elements in steels are classified in two groups: alpha-stabilizers (i.e. Cr, Si, Mo…), which increase the temperature for the transformation, or gamma-stabilizers (i.e. Ni, Co, Mn…), that decrease the temperature for the transformation.

The processes described above represents that what appears in the phase diagram, where a quasi-equilibrium state is required. That means slow cooling rates that leave time to atoms to diffuse; carbon is expel from transformed ferrite, partitions, and must travel to austenite; iron must rearrange from FCC to BCC, and finally austenite must decompose in two different components. The fact that this process needs time, means that different cooling rates can lead to different dynamics of transformation. This is what makes steels extremely versatile.

Annealing is a thermal process that involves giving the metal energy by increasing the temperature, so microstructure evolves closer to equilibrium. During annealing there are different stages depending on the temperature reached. First thing that happens is the accommodation and annihilation of dislocations and internal stresses, which leads to the softening of the material and is usually applied before forming the material or in other to reduce the effect of work hardening after cold deformation; this stage is known as recovery. After that, recrystallization takes place. New strain-free grains nucleate from those highly deformed, which leads to fine and equiaxial grains. Last stage involves grain growth: grain size increases because the specific plane orientations take preference over others. Therefore, in grain boundary, were two orientations coexist, atoms will jump from one to another following minimum energy criteria [13]. Most annealing processes aim to homogenize the structure and soften the material, and typically avoid reaching austenization temperature.

1.2.1 Martensitic transformation

Quenching is a heat treatment performed in metals that consists in taking the alloy to high temperature where a phase transformation takes place, followed by rapid cooling.

This is applied to several metals as titanium alloys [14], but it is mostly used in the steel industry.

In steels, quenching is performed from total or partial austenization and cooling down to room temperature. Typically, the result of this process is a carbon supersaturated tetragonal ferrite with lath or plate like martensite microstructure.

In martensite, carbon atoms in supersaturated ferrite locate in interstitial octahedral positions if the BCC lattice and get ordered in a preferred direction, which leads to a deformation in a certain axis. Therefore, martensitic ferrite structure is not BCC, but is BCT (Body Centred Tetragonal) [6]. Bain proposed a model to explain this by displacive theory, where iron atoms do not diffuse but rearrange in a military way so that shifting lattice angles same neighbouring atoms go directly from FCC order to BCT [15]. As it is shown in Figure 5, an FCC structure as austenite, with lattice parameter a_γ contains itself a BCT structure with base and height lattice parameter a_α and c_α, respectively.

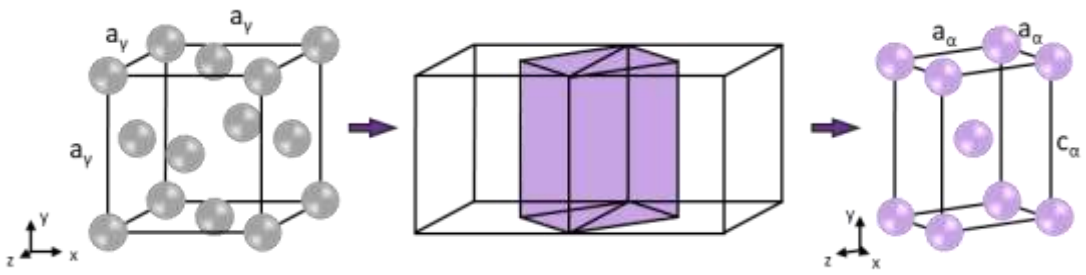

Figure 5. Bain model for martensitic transformation [16]*. a_γ is the lattice parameter of the FCC austenite, a_α and c_α are the lattice parameters of the BCT ferrite.*

According to this scheme, γ FCC vertical compact planes $(1\ 0\ 0)$ and $(0\ 0\ 1)$ correspond to α BCT $(1\ 0\ \bar{1})$ and $(1\ 0\ 1)$ respectively. And lattice parameter cα is equivalent to aγ and aα is equal to $\sqrt{2}/2$ cα. Tetragonality of the BCT lattice is measured by c/a value which in this case is 1.4142. After this transformation, lattice relaxes due to minimum energy accommodation by means of elastic strain. Final tetragonality depends on the carbon supersaturation of the ferrite, in the case of 2.8% at. c/a = 1.03 [17]. When there is no carbon supersaturation, or it is randomly distributed, this value would drop to 1 and lattice would be BCC again.

Carbon occupies octahedral interstitial positions along the lattice, in FCC it corresponds to body centred and edge positions, but in BCC it corresponds to unit cell edges. Those positions can be oriented in x, y, or z, but during this transformation a certain orientation stands out with lower free energy than the others, longitudinal direction, probably due to the presence of carbon positioned there already. Then, driving forces are generated for

carbon to occupy adjacent positions of this preferred direction so forces the tetragonality of the lattice.

Since these treatments are performed in out of equilibrium conditions, phase diagrams no longer represent the phenomena that is taking place. To study kinetic of phase transformation CCT (continuous cooling transformation), Figure 6, and TTT (temperature-time-transformation), Figure 7, diagrams should be used for continuous cooling and isothermal treatments, respectively.

In the CCT diagram below, Figure 6, we can observe the different microstructures that can be obtained by continuous cooling in a certain steel. Starting from the austenization temperature, A_3, martensite is formed at rapid cooling rates, quicker than 200ºC/s approximately. At lower rates, other structures can appear too. Pearlite instead is formed at cooling rates lower than 25ºC/s. Temperature at which martensite starts to form is known as M_s and in this case, it would be around 460ºC; A_1.

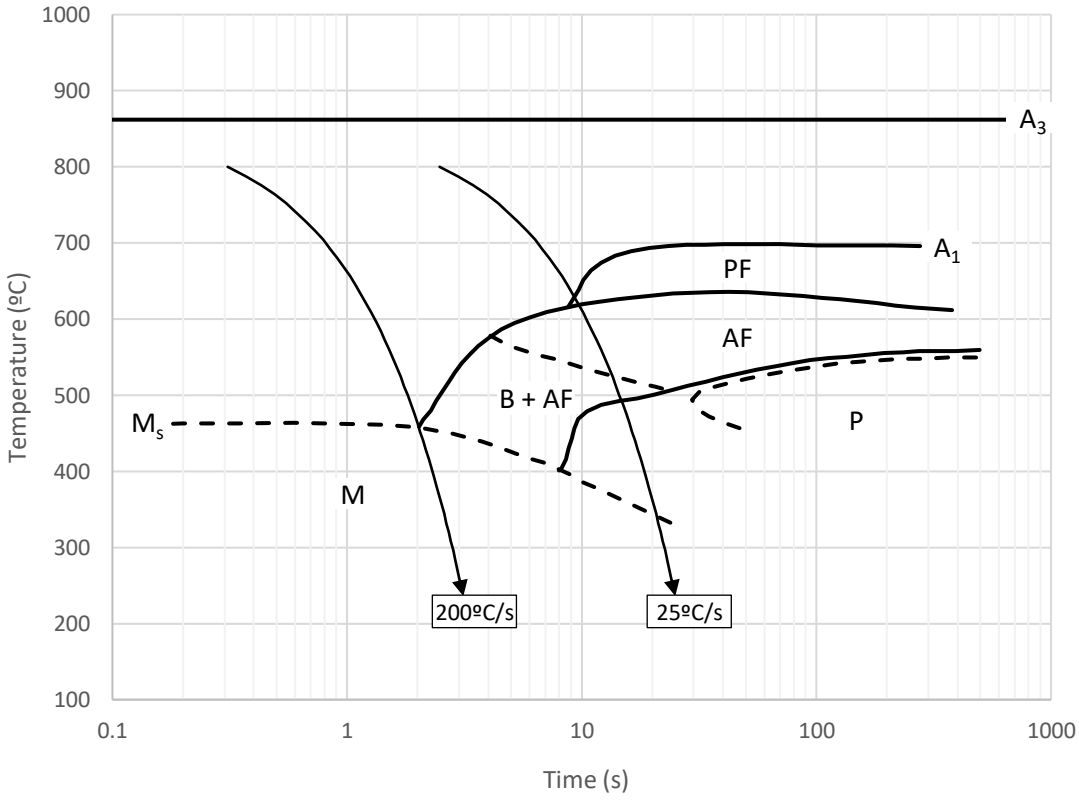

Figure 6. CCT diagram for 0.12C-0.8Mn-0.25Si (wt%). Relevant temperatures are designated as A_3 for austenization, A_1 for the ferritic transformation and M_s for the martensitic formation. Structures featured are: poligonal ferrite (PF), acicular ferrite (AF), pearlite (P), bainite (B) and martensite (M). Adapted from [18].

Martensite growth is formed as an acicular structure (needle–like shape) or laths. The displacive nature of this transformation leads to high internal deformations and dislocations density contribute to making this phase –and steels containing it– extremely hard. But it also makes martensitic steels extremely brittle and difficult to work with. Because of this, martensite is usually tempered after being quench. Tempering is a specific heat treatment that relaxes internal stresses in martensite reducing dislocations density and tetragonality and helps with transforming part of retained austenite to other phases.

For specific cooling rates between those required for martensite and pearlite, a distinct structure is formed, known as bainite.

1.2.2 Bainitic transformation

Bainite microstructure is found in ferritic steels after isothermal treatments at certain temperatures. These consist of austempering and partial quenching down to the selected temperature to prevent transformation at higher temperature [19]. The treatment temperature for bainite formation is among M_s and B_s, represented in Figure 7.

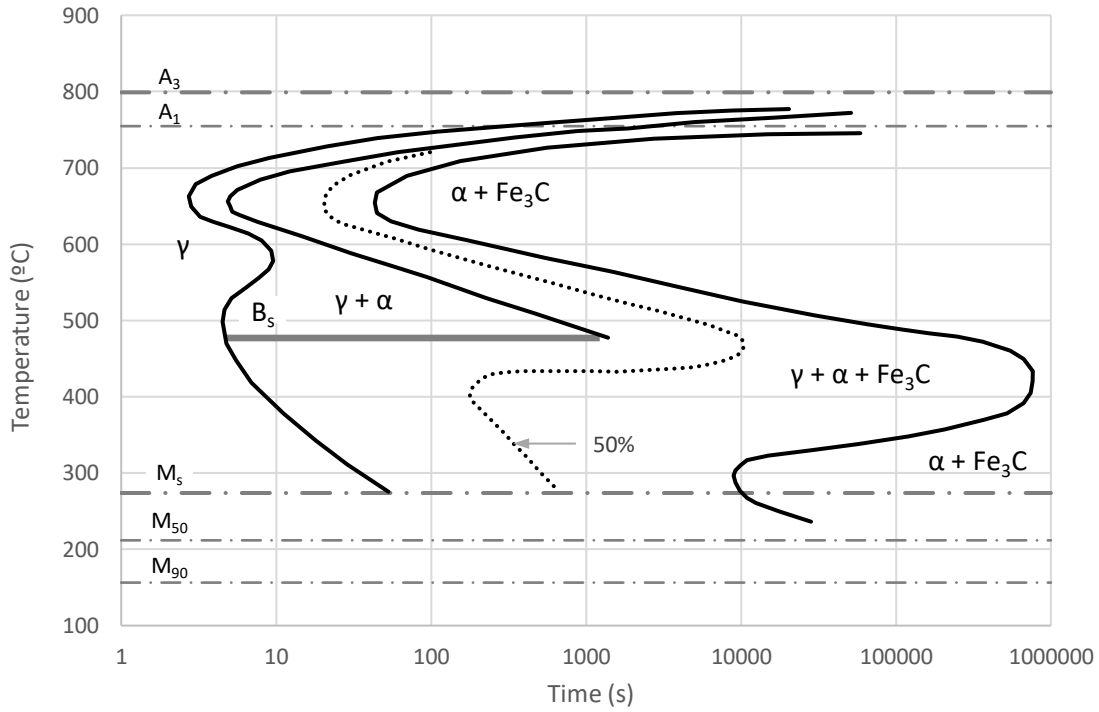

Figure 7. TTT diagram for 0.55C-1.6Si-0.77Cr steel: A_1 and A_3 stands for austenization start and end temperatures; B_s for the highest temperature at which bainite forms; and M_s, M_{50}, and M_{90} for martensitic transformation temperatures. It features phases instead of microsctructures. Adapted from [20].

In TTT diagrams as the one shown in Figure 7, curves represent in which moment in time transformations take place depending on temperature the treatment is kept. The

steel to which this diagram corresponds to is a hypoeutectic composition. From left to right, first line corresponds to the starting of ferrite formation; second curve indicates the point of the eutectoid transformation, dots line marks the point where half of γ have been transformed into α or cementite; and last curve indicates when austenite transformation is concluded.

In the present case, formation of perlite in isothermal treatments takes place from 755ºC (A_1) to 470ºC. This temperature is known as B_s and points the maximum temperature at which bainite structure is observable. This is a structure appearing in steels given isothermal treatments typically between 125ºC and 550ºC [21].

Bainite was first observed back in 1920's by Edgar Bain, who proposed the name martensite-troostite, as what he interpreted as an intermediate structure of martensite and troostite (name used then for fine pearlite). It was not until 50's that it started to be named after himself, as we know it.

There has been a fierce discussion over the last decades among the metallurgist community on whether bainite is formed via reconstructive or displacive transformation [22].

Reconstructive theory says that when temperature drops below A_1 and austenite becomes unstable, ferrite formation nucleates and advances in a similar way to the formation of Widmanstätten ferrite [23]: iron atoms throughout grain boundary (where lack of order elevates free energy) detach from austenite and rearrange in ferrite lattice. In the meantime, carbon is mostly kept in austenite (where it is more stable) balancing carbon content in ferrite until remaining austenite reach supersaturation and carbides start to precipitate. Displacive theory, on the other hand, says that ferrite formation occurs in a similar way to martensitic: iron atoms do not diffuse but FCC lattice shifts to BCC conserving atomic neighbours and plains as Bain model explained. In this case, transformation is instantaneous and ferrite conserves carbon content [24]; in the case of higher bainite, higher temperature prevents instant transformation and carbon diffuses from ferrite to austenite, increasing its concentration as transformation progresses and forms carbides between ferritic laths; in lower bainite the process is similar, but carbon partitioning is not completed and some is left in the ferrite which leads to carbide precipitation inside plates [25]. In brief, reconstructive theory affirms that iron diffusion controls the transformation; displacive theory denies iron diffusion affects the transformation. However, the latest contributions in this scientific field have incorporated new evidences that support the displacive nature of this process [26].

The traditional heat treatment to produce bainite is known as austempering. As it has been said earlier, it starts by heating up steel over austenization temperature, A_3, until

homogeneous transformation is achieved in the sample. Then the sample is cooled to the selected isothermal treatment temperature, cooling rate must be sufficiently fast to prevent any transformation before reaching this point. Afterwards, temperature is kept until fully transformation has happened according the TTT chart; in example, the steel for which TTT in Figure 7 was made, would require austempering at 400ºC for more than 1800 hours for fully bainitic structure.

Austempering is a time and energy consuming process that carries a high cost for the industry. This is because depending on the size of the piece and the composition of the steel, it requires long furnace times, for some compositions up to several days, and that requires a lot of energy even for intermediate temperatures treatment. The current trend in the research of these material is focused on improve the process by reducing the temperature required, B_s (bainite transformation starting temperature), i.e. adjusting the composition in substitutional solutes [27]; and shortening the time it take to transform, i.e. increasing nucleation sites as proven by ausforming (applying deformation at the beginning of the austempering) [28].

Bainite is hierarchically structured. Bainitic ferrite plates stack parallel, usually separated by other phase as austenite or cementite. Stacks of parallel plates are known sheaves and share the same crystallographic orientation. A sheave comes from each nucleation, typically from prior austenite grain boundary and is wedge-shaped into the grain. Sheaves coming from different nucleation but from the same prior austenite grain share a common set of crystallographic orientation related to that of the prior austenite [24].

According to the temperature at which the austempering treatment is performed, it can be described two different microstructures of bainite: upper and lower bainite. Upper bainite is formed at higher temperatures, closer to B_s, where carbon diffuses away from ferrite as it forms, then it is surrounded by larger carbon-rich austenite. Final structure consists in carbide free ferrite surrounded by carbon-rich phases as austenite, cementite or even martensite. Lower bainite forms at lower temperatures, closer to M_s. At this temperature carbon diffusion drops and gets caught inside ferrite. Carbon supersaturation in ferrite leads to later precipitation of carbides inside the ferrite [29].

Carbides present in upper bainite are usually cementite but for some exceptions [24]. On the other hand, carbides presence inside lower bainite are not clear. These carbides precipitate in a temperature range in which diffusion of carbon is highly restricted, that leaves carbon distribution of different stages of carbide precipitation [30].

2. OBJECTIVES

As previously stated, microstructure is directly related to mechanical behaviour of metals. Material properties as hardness depend on the phases present in the microstructure and how they arrange; if there are precipitates and what type, where are they located, how are they shaped; grain size and orientation, dislocation density, etc.

This is highly interesting for alloy design since composition is calculated to optimize the microstructure. However, a certain alloy can show different microstructures leading to different properties. Microstructure can be modified mechanically and thermally –or by combining these two methods.

In this case, we are interested in the effect of different heat treatments on the microstructure of a steel. Displacive nature of martensitic and bainitic transformation generates internal stresses, deformation associated to lattice shifting needs to accommodate plastically in surrounding austenite which leads to high dislocation density and stacking faults [31]. In the case of quenched martensite, tempering relaxes the material improving toughness [32], but also aids carbon diffusion allowing carbide formation and breaking up supersaturated austenite that could transform into extremely brittle martensite. In the case of lower bainite, microstructural factors that control properties such as hardness and strength are plate thickness and dislocation density and carbides within [33]; elongation is controlled mainly by the amount of retained austenite [34].

Regarding carbon distribution, formation of martensite during quenching freezes carbon distribution from austenite, but tempering aids carbon diffusion and allows nucleation of carbon rich phases; austempering does not prevent carbon movement, but in lower bainite it is still very restricted and is only due to the long exposure times that carbon can segregate towards austenite or nucleate carbides as cementite in the ferrite matrix.

It can be assumed that during austenization carbon distribution is perfectly uniform and it adjusts to mean composition of the steel. Following carbon segregation that leads to enrichment at certain areas can be described as a step-by-step process by which different characteristic compositions form one after another progressively before reaching a final equilibrium.

Rementeria et al. [17], who carried out analyses by Atom Probe Tomography, APT, in different bainitic structures of high-silicon high-carbon steels, revealed several of these intermediate metastable phases. According to the results, carbon distribution in bainitic ferrite shows four distinguishable states shown in Table 1.

Table 1. Carbon content and stoichiometry of precipitation stages in low bainitic ferrite in a steel with 2.96% atomic carbon content [17].

C_{α} (%at.)	C_{disloc} (%at.)	$C_{cluster}$ (%at.)	$C_{carbide}$ (%at.)
0.22%	15%	10.90%	25%
-	-	$Fe_{16}C_2$	Fe_3C

Although the steel contains 2.96 atomic percent carbon, bainitic ferrite matrix only conserves 0.22% despite being the most abundant phase. Some carbon could have partitioned into the retained austenite, which makes up to 17% of material volume, but the rest is in form of carbon rich precipitates. APT analysis showed cementite, Fe_3C, and dispersed clusters with 10.90% carbon content corresponding approximately to the stoichiometry of $Fe_{16}C_2$. Also, isoconcentration surfaces of 15 at. % showed carbon segregation towards elongated shapes thought to be dislocation, which due to the slight disorder increase tends to trap solute.

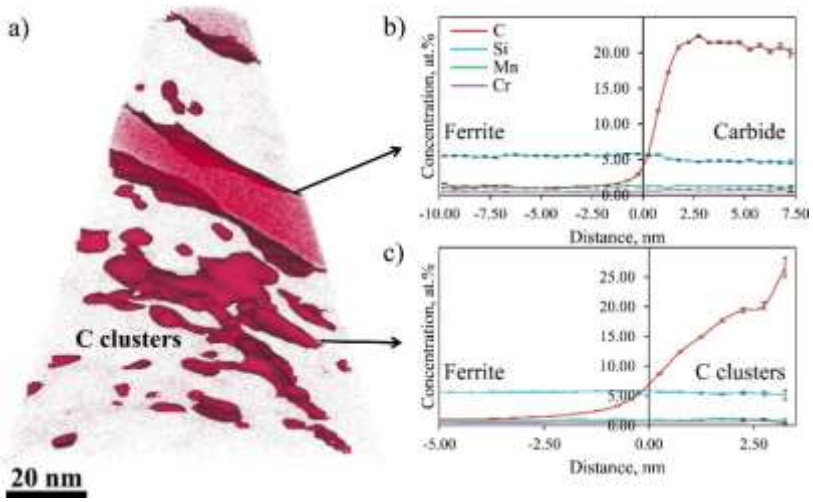

Figure 8. a) 3D map of carbon in a 1 wt.% steel austempered at 250ºC obtained by APT, isoconcentration surfaces for 7% at.%; b) and c) represent concentration of C, Si, Mn and Cr through isoconcentration surfaces indicated by arrows [35]. *Courtesy of R. Rementeria.*

This could demonstrate that the segregation of carbon does not occur in a continuous and homogeneous way but is produced by grouping atoms in the form of clusters and

around defects. In addition, another important part of the carbon expects to be partitioned into the retained austenite, which makes up 17% of the volume of the material.

One of the most important limitations for industry is the heat treatment required to achieve the desired properties of the material. Optimizing procedures like these is vital to the progress of technology. Therefore, it is important to have as deep knowledge as possible about the internal processes that occur during the heat treatment and the physics behind them.

This work aims to compare the microstructures obtained by different isothermal heat treatments on the same steel. The treatments selected for such comparison will be austempering and quenching-tempering. And to allow an effective comparison, the temperature of the isothermal treatments will be the same in both cases. We will focus on the effect related to the deformation caused by the accommodation of both displacive transformations, and the differences in the carbon distribution.

3. MATERIALS AND METHODS

3.1 Materials

The base material for this project was provided by the National Center for Metallurgical Research of Spain (CENIM – CSIC).

3.1.1 Composition

The material choice is a high-carbon high-silicon steel alloyed with additional elements [27]. In this case carbon has a role in lowering the bainitic transformation temperature and increasing the retained austenite volume [31]; silicon stabilizes carbon rich austenite preventing its transformation [31]; manganese and chromium ease steel quenching preventing the formation of proeutectoid α; nickel is used in steel improving toughness; and molybdenum is commonly found to prevent embrittlement caused by impurities precipitation in grain boundary [36]. Composition can be found in Table 2.

Table 2. Chemical composition for the studied material.

	Fe	C	Si	Mn	Cr	Ni	Mo
wt%	Balance	0.66	1.45	1.35	1.02	0.09	0.24
at%	Balance	2.96	2.78	1.32	1.06	0.13	0.13

3.1.2 Heat treatments

To compare the effect of the process in the selected steel two different treatments were selected: quenching and tempering for martensitic structure, and austempering for bainitic structure. Those treatments were carried out in the controlled furnace of the dilatometer described below.

B220 stands for austempered samples and M220 stands for quenched and tempered samples. Both heat treatments start austenizing the steel at 900ºC, slightly above A_3, for 15 minutes (longer times would cause unwanted grain growth). At this point, M220 samples were quenched to room temperature, while B220 samples were quenched to 220ºC and kept for 8 hours for the isothermal part of the process. M220 samples, after 10 seconds at RT, were tempered at 220ºC for 1 hour. In all cases the heating rate of 5ºC/s and cooling – in this case, quenching – at 50ºC/s, Figure 9.

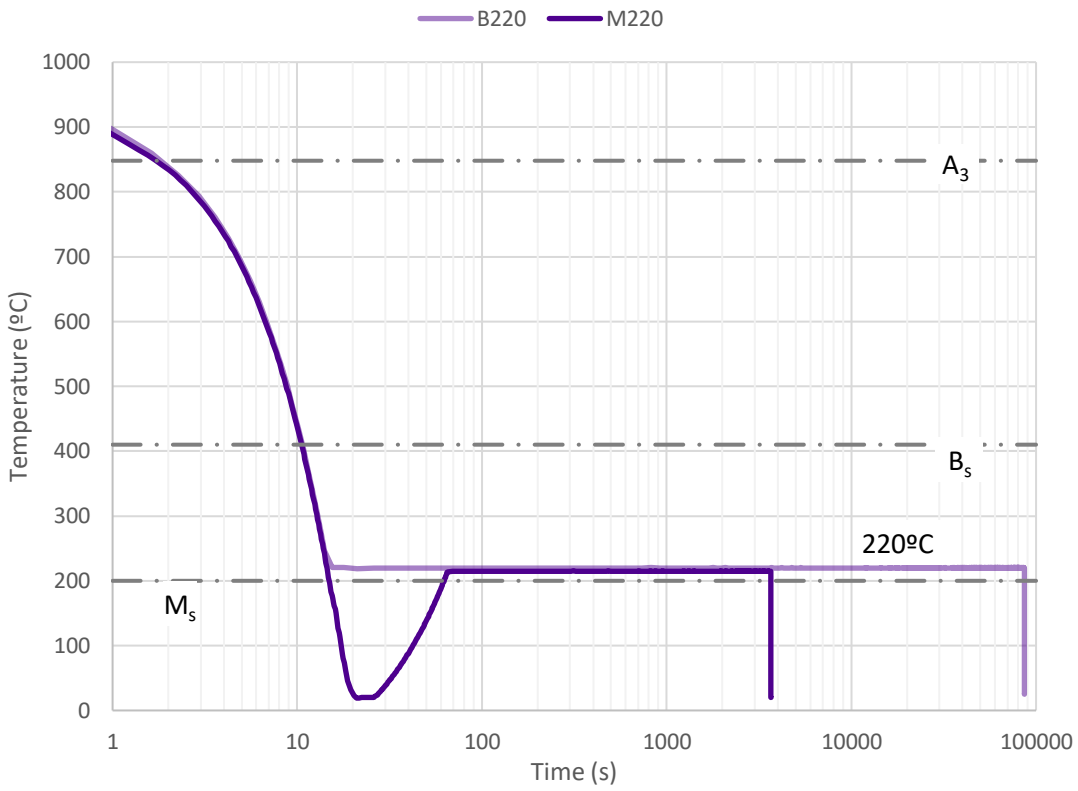

Figure 9. Each of the heat treatments performed for this study.

An additional sample named MART, that correspond to a similar quench than M220 but without tempering, was prepared for XRD analysis.

3.2 Methods

3.2.1 Dilatometry

As said earlier, the transformation parameters of the steel were studied by dilatometric analysis at CENIM facilities. Those parameters are needed to understand how the transformation takes place and design the heat treatment to control the final microstructure.

Dilatometric analysis allows monitoring the phase transformation of steel during different thermal cycles. This technique consists in measuring the volume of a sample as a function of temperature. In the case of steels, eutectoid phase transformation goes from solid to solid, but lattice structure conversion involves a change in the specific volume [37].

Typically, specific volume is proportional to temperature due to regular thermal expansion; in the case of a phase transformation, atomic packaging difference will be seen as a sudden shift in specific volume, and different phases with different expansion coefficients will show different slopes. More compact phases like Face Centered Cubic or

Hexagonal Close Packed will have lower specific volume like Body Centered Cubic, for example. In this test, the dilatometer applies heat or cools to the sample in an inert atmosphere controlling the temperature, while at the same time measures the evolution of length.

Analyses were carried out using an Adamel Lhomargy DT1000 – computer controlled high resolution dilatometer – at CENIM physical metallurgy laboratory. The tests are performed in a controlled vacuum or inert atmosphere, to prevent oxidation or decarburization, in a small sample chamber. Temperature is measured with a type K thermocouple welded directly to the sample. Heating is controlled by a double tungsten filament radiation furnace incorporated to the chamber; cooling is controlled by a servo-valve released helium flow which in turn can be cooled with a liquid nitrogen heat exchanger if needed. An amorphous silica pushrod transmits length variations to a Linear Variable Differential Transformed (LVDT) sensor [37]. All this translates into an excellent heating/cooling rate from 0.003 to 500 K/s.

3.2.2 X-ray diffraction (XRD)

X-ray diffraction, XRD, analysis had been carried out to determine: austenite volume fraction, V_γ; lattice parameter of austenite, a_γ; and lattice parameters of bainitic ferrite, $a_{\alpha'}$ and $(c/a)_{\alpha'}$, using Rietveld method [38]. Then, lattice parameters have been used to estimate lattice parameters, carbon content on austenite [39] [40], and bainitic ferrite [41][42].

XRD experiments were performed at CENIM – CSIC X-ray characterization laboratory [43] [44]. The equipment used was a Bruker AXS D8 diffractometer equipped with Co-K_α X-ray tube, Goebel mirror and Lync Eye Linear Position Sensitive detector. Diffraction patterns data collected included 2θ from 35º to 135º and a step size of 0.015º [45].

3.2.3 Scanning transmission electron microscopy (S-TEM)

The main technique we used to carry out the analysis of the samples is transmission electron microscopy. This technique has been performed at Tampere Microscopy Center (TMC), at Tampere Universities (TAU).

The transmission microscope Jeol F200 S/TEM, at TMC, was used to obtain bright field (BF) and dark field (DF) TEM images, and selected area electron diffraction (SAED) patterns. Treatment of the images was performed using GMS.3 Gatan commercial software. [35].

A main concern of the preparation of these samples was the magnetic nature of the material, and undesired interaction they could have with the electron beam, due to the electrical charge nature of this. This could have produced noise, deform the patterns, and lead to errors in measurements. Therefore, to minimize the negative effect of this situation it was required to reduce the amount of material, producing slices as thin as possible, and symmetry to avoid the predominance of a certain magnetic domain [46].

Table 3. List of the electrolytes tested for dual jet electropolishing.

Name	$HClO_4$	Glycerine	Ethanol	HNO_3	Methanol
Perchloric	5%	15%	Balance	-	-
Nital-21	-	-	-	21.67%	Balance
Nital-16	-	-	-	16.25%	Balance
Nital-13	-	-	-	13%	Balance

Sample preparation was done in TMC laboratories. Thin disks were obtained by slicing the dilatometer size samples, Ø3mm and 10mm long cylinders, and then grinding, polishing to obtain Ø3mm and 100µm thick disks. To achieve TEM suitable thickness, (~100nm), disks were thinned by dual jet electropolishing using a Struers TenuPol-5. Samples were polished until a hole was performed, triggering an infrared light detector. Several electrolytes with different pH were tested and compared; finally, the best results were achieved using Nital-21 from the list above, Table 3. Operating voltage used was 12V and electrolyte was cooled in ethanol/liquid nitrogen bath to -30ºC [46].

4. RESULTS

4.1 Phase transformation

In Figure 10 there is the plotted results of a dilatometry test of the studied material, first, heating from RT to 900ºC at 5ºC/s; then, cooling back to RT at 50ºC/s. There we can observe a constant expansion during the heating up to around 793ºC, where a sudden drop in length indicate the austenitic transformation had started (A_1). Expansion is restored at 848ºC, which is an indication that transformation has concluded, and the steel is fully austenite (A_3), the phase change is indicated with dash line. After reaching 900ºC cooling start, rapid cooling keeps austenite untransformed until just before 200ºC, where sudden and quick expansion indicates the starting of the martensitic transformation (M_s).

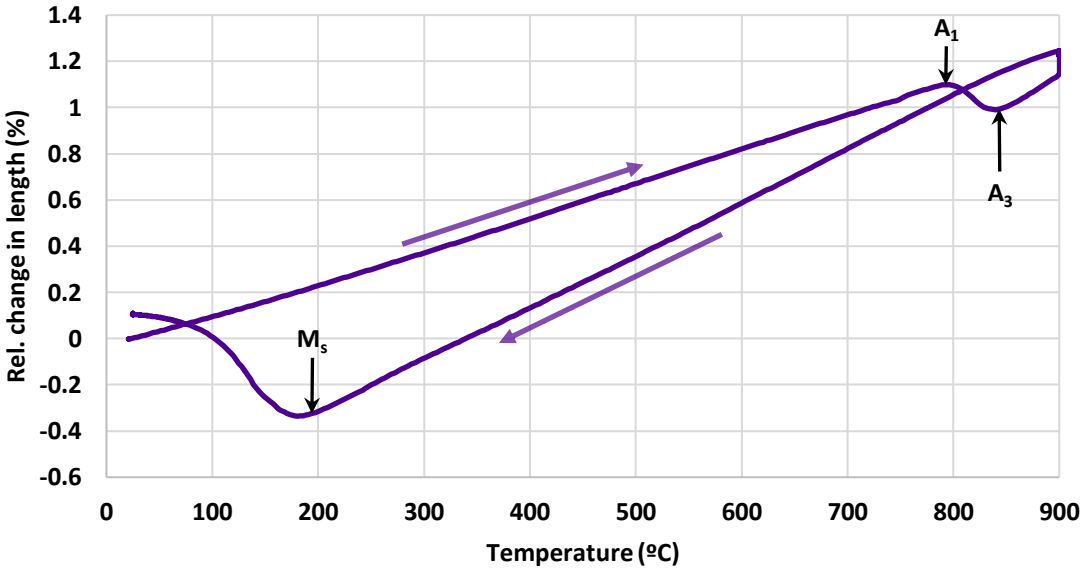

Figure 10. Dilatometric test perfomed to studied steel. Temperatures of start (A_1) and finish (A_3) of the austenization and martensitic transformation (M_s) can be resolvable by the sudden variation in length.

Phase stability and volume fraction at different temperatures was estimated by thermodynamic model-based tools (ThermoCalc) [43]. Austenization temperature (A_3) and martensite transformation temperature (M_s) were determined by dilatometric analysis. Whereas, bainitic transformation starting temperature (B_S) was calculated by compositional based model [47]. These transformation temperatures are summarized in Table 4.

Table 4. Relevant transformation temperatures for the studied material.

A_3	B_s	M_s
848ºC	410 ºC	200 ºC

4.2 X-Ray diffraction results

X-ray diffractometry was used to characterize the phases in the samples. Diffraction patterns were fitted using Rietveld method to calculate volume fraction, as well as the lattice parameters [38]. Using these values, we could calculate the strain and carbon content of each sample: austenite cubic lattice parameter, a, depend on carbon in solid solution as ferrite tetragonal a/c relation.

Table 5. Data from XRD parameters.

Sample	$\mathbf{V_\gamma}$ ±2%	$\mathbf{c/a_\alpha}$ ±0.0004	$\mathbf{C_{\alpha'}}$ (wt.%) ±0.008	$\boldsymbol{\varepsilon_\alpha}$ ($\times 10^{-3}$) ±0.2	$\mathbf{a_\gamma}$ ±0.008	$\mathbf{C_\gamma}$ (wt.%) ±0.008	$\boldsymbol{\varepsilon_\gamma}$ ($\times 10^{-3}$) ±0.2
MART	13.52%	1.0211	0.485%	3.7	3.59009	0.794%	2.3
M220	15.76%	1.0086	0.197%	2.3	3.59524	0.921%	2.8
B220	19.20%	1.0085	0.194%	2.4	3.60668	1.196%	2.2

V_γ is de volume fraction of austenite, **c/a_α** is the relation between lattice parameters that represents tetragonality in ferrite, **a_γ** is the lattice parameter of austenite, **C** is the carbon content of each phase calculated from c/a_α and a_γ respectively, and **ε** is microstrain in each phase.

These results are summarized in Table 5, MART sample correspond to the M220 before tempering. MART shows less austenite than M220, but it is within the error, therefore, there is no significant formation of austenite during the tempering; what is notorious is the reduction of carbon content within the ferrite and the relaxation.

B220 sample corresponds to the austempered steel. The pattern of this sample was fitted including an additional FCC phase corresponding to a slightly different austenite. This is because of in this sample we usually find two main austenite morphologies: laminar when it remains between ferrite plates, and blocky when it is trapped between different sheaves. That causes that lamellar austenite receives more carbon from transforming ferrite than blocky does, causing larger lattice parameter - blocky austenite contains only 0.94wt.% carbon whereas lamellar contain 1.41wt.% carbon.

Furthermore, given the volume fraction and carbon content of each phase, we can calculate the total quantity of carbon in solid solution. Assuming that the rest of the carbon is in the form of precipitation, we can estimate the volume of precipitates formed in the alloys. According to these calculations, MART samples retain most of the carbon in supersaturated ferrite, only 20% of the carbon in the steel is in precipitates; at M220, on the other hand, over 50% of carbon had precipitated during the tempering; B220 show 42% of carbon in precipitated.

In addition, XRD can estimate the residual elastic stresses, e. And considering that the samples have been analysed after the treatments, any internal deformation must come from the phase transformation. The sample with the higher e_0 is MART, ferrite retain most of the deformation during its accommodation in the structure, while M220 ferrite got relaxed during the first stages of tempering; austenite is not so affected. In the case of B220 sample, e is in the range of M220.

4.3 TEM observations

To observe the microstructure of the treated samples, we used Transmission Electron Microscopy (TEM).

In Bright Field (BF) TEM images, the contrast obtained is from lattice orientation. This is diffraction contrast, grain with orientations that satisfies Braggs law appear darker than those whose orientation interacts less with the electron beam. Also defects in the lattice such as dislocations will appear darker because produce higher absorption. Other dark features can correspond to precipitation, cementite in this case, or higher concentration of solute elements.

Conversely, in Dark Field (DF) TEM images, orientation contrast highlights wherever the misorientation is higher. Therefore, where Braggs law is satisfied appears bright.

Finally, if something looks dark in both bright and dark field, it is because the absorbance there is higher and therefore the electron beam neither passes through it nor is diffracted. This may be due to the thickness being greater, for example if it is a precipitate that is more resistant to electrochemical attack; it may be because the composition is enriched in heavier elements; Or it may be because the disorder is greater and has an effect of trapping and dispersing the electrons.

Austempered samples, B220, showed bainite structure, characterized by bainitic ferrite (α_b) disposed in parallel plates and retained austenite (γ_r). According to the XRD results,

Table 5, it is calculated that a 17% of the volume consists of austenite. Figure 11 shows two different BF-TEM images from different areas of B220 microstructure: in *a*, we can identify bainitic plates due to the diffraction contrast by which they look brighter, while austenite appears to be darker; in *b*, we see similarly α and γ, but also, we can see some darker spots along the ferrite. Those could be caused by precipitation of cementite – as it would be expected in lower bainite – or could be caused by tangles of dislocations.

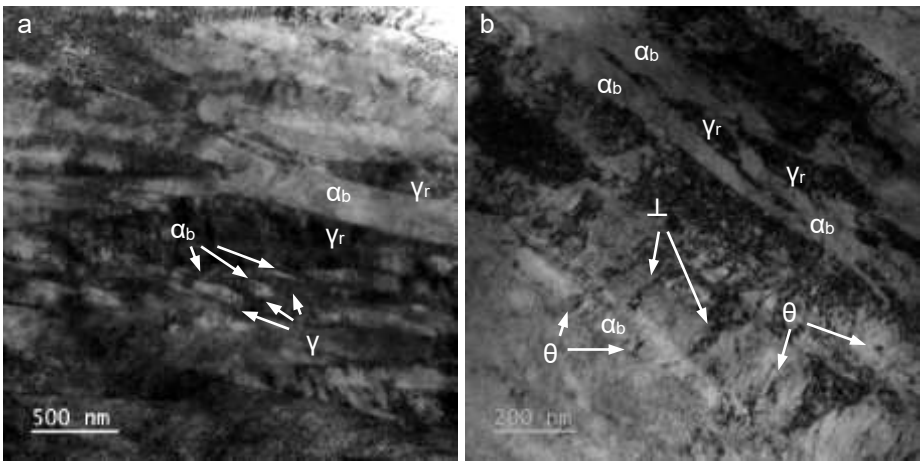

Figure 11. Bright field TEM images of representative areas of bainitic structures in B220. Phases featured are bainitic ferrite, α_b; retained austenite, γ_r; and cementite (Fe_3C), θ. ⊥ points at dislocations forests.

In the case of tempered and quenched samples, M220, the microstructure corresponds to a martensitic steel. The structure of ferrite in martensitic sample (α') is very similar to what was found in the bainitic sample. Figure 12 shows a lath of bainitic α', its orientation makes it dark in BF and bright in DF due to the diffraction contrast; Figure 12c represents the Selected Area Electron Diffraction (SAED) pattern obtained in the interior of the lath from the previous images, which corresponds to [001] zone axis of BCC lattice – SAED patterns do not appreciate tetragonality.

Figure 13 corresponds to a α' lath where a SAED analysis has been performed. Pattern obtained present the overlapped spots of both BCC *[113]* and *[110]* zone axis. That means that concurs with different ferrite sheaves and therefore share variants.

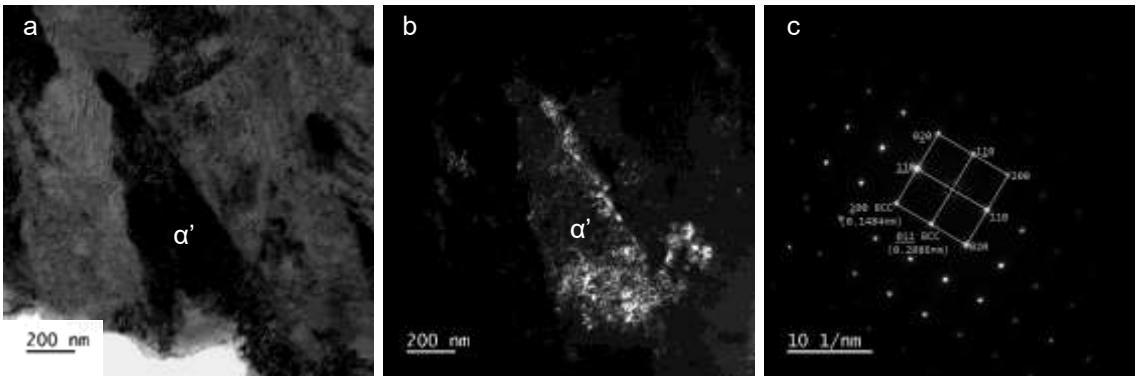

Figure 12. a) BF-TEM image of a α' lath in M220; b) DF; c) the SAED pattern from the interior of the previous lath, zone axis [001].

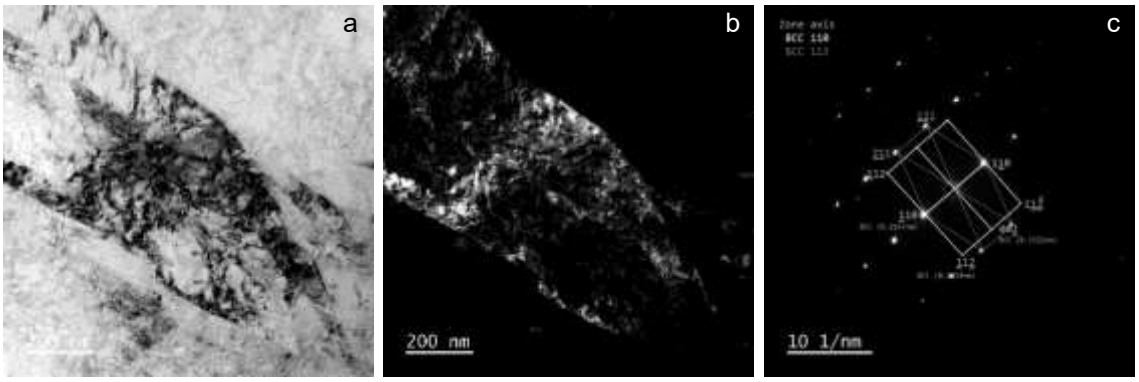

Figure 13. a) BF-TEM micrograph of a α' lath in M220 sample, b) DF-TEM micrograph corresponding to the same area; c) SAED pattern indexed for [110] zone axis (brighter) and [113] (darker).

4.3.1 Carbon distribution

We can assume that carbon is homogeneously distributed in throughout the material during the austenization step of the thermal cycle of both materials. Once the M220 is quenched, carbon should have had very little time and energy to diffuse and therefore carbon that did not partitioned – most of it – is still trapped in martensitic ferrite. But shortly after, tempering treatment reactivate carbon mobility allowing it to diffuse to γ and/or form more stable configurations, such as carbide. In a similar way, when B220 gets cooled to isothermal treatment temperature, carbon mobility gets severely reduced: some carbon partitions to γ, stabilizing it at lower temperature; some carbon gets stuck at bainitic ferrite where clusters and precipitate over the course of the treatment.

In the case of these steels, high-silicon content stabilizes austenite with high carbon concentration preventing its decomposition into ferrite and carbides, but carbides can still form from carbon supersaturation of ferrite.

From Rementeria's work on carbon distribution on B220 steel through in-situ synchrotron X-ray characterization, found out the formation of cementite and η-carbides during austempering process [35]. On the basis of APT results of Rementeria et. al. [44], we know that carbon in bainitic ferrite segregates into dislocations and aggregates in homogeneously dispersed of $Fe_{16}C_2$ stoichiometric ordered clusters leaving a carbon-depleted bainitic ferrite matrix [17] before evolving into carbides with higher carbon concentration. According to thermodynamic based models predictions, these clusters corresponds to α'', an ordered tetragonal phase which consists in $Fe_{16}C_2$ [49].

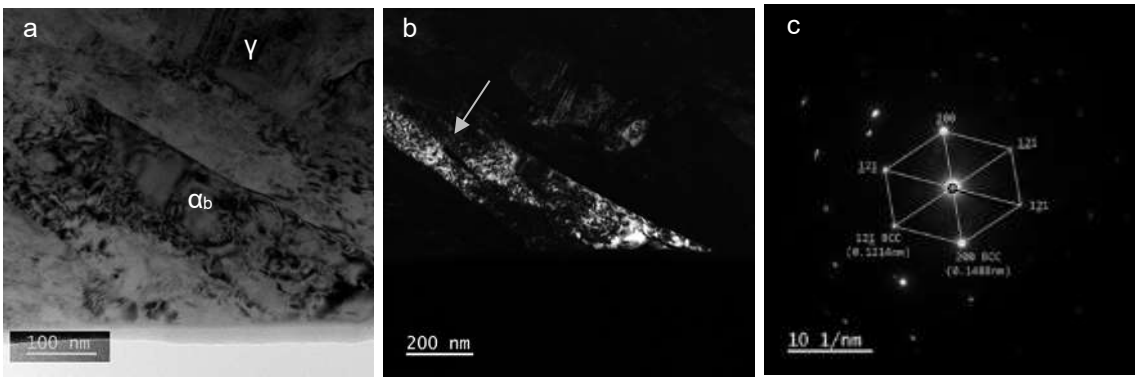

Figure 14. a) BF-TEM image of a B220 sample; b) DF-TEM image of the same area; c) the SAED pattern corresponding to the interior of the plate in a) and b), zone axis [012].

In the context of this work, both samples have been investigated looking for carbide formation. Figure 14 is a representative image of B220 microstructure. Although SAED pattern is not conclusive, DF image shows an anomaly that resembles cementite precipitate [35].

Figure 15 shows a lath of martensitic ferrite in M220 steel with carbide precipitates. This precipitation seems to have nucleated at prior austenite grain boundary, following a specific crystallographic orientation for each of the sides. Which leads to the formation of parallel longitudinal precipitates.

Each set of cementite corresponds to different, yet equivalent, crystallographic variants on the ferrite which, due to the displacive nature of the transformation, is inherited from prior austenite leading to symmetric precipitation.

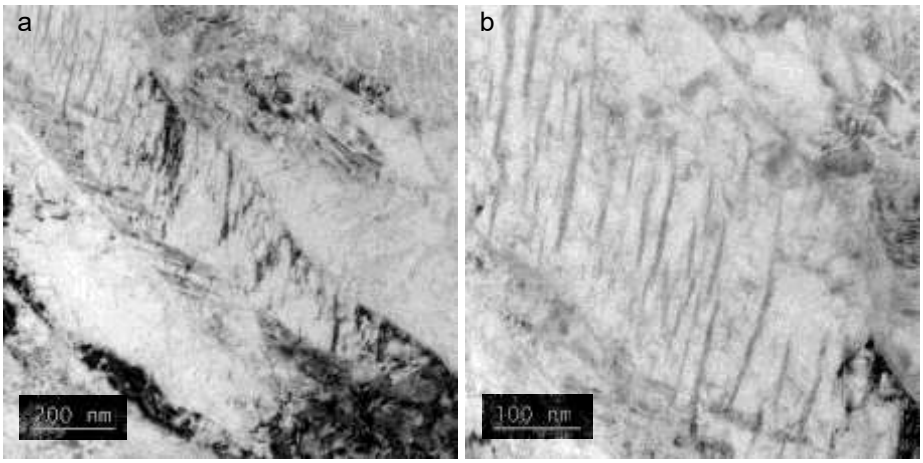

Figure 15. BF-TEM micrographs of a M220 sample.near to where Figure 13 was obtained, a) display a martensitic lath in which longitudinal precipitates can be noticed; b) display those precipitate at higher magnification.

Although this kind of precipitation has been seen frequently throughout the examined sample, most of the microstructure presented precipitate free martensite. Figure 16 presents a different ferritic lath where there are no distinguishable precipitates through bright nor dark field TEM images. SAED pattern correlates to BCC lattice with $[111]$ orientation. In this SAED pattern, we found the presence of satellite-like spots at some of the (011) plane family towards $[0\bar{1}1]$ direction. Similar spot satellites have been associated to the formation of secondary lattices corresponding to nanoprecipitation of ordered clusters, in this case, $Fe_{16}C_2$ carbon clusters previously reported in B220 [17].

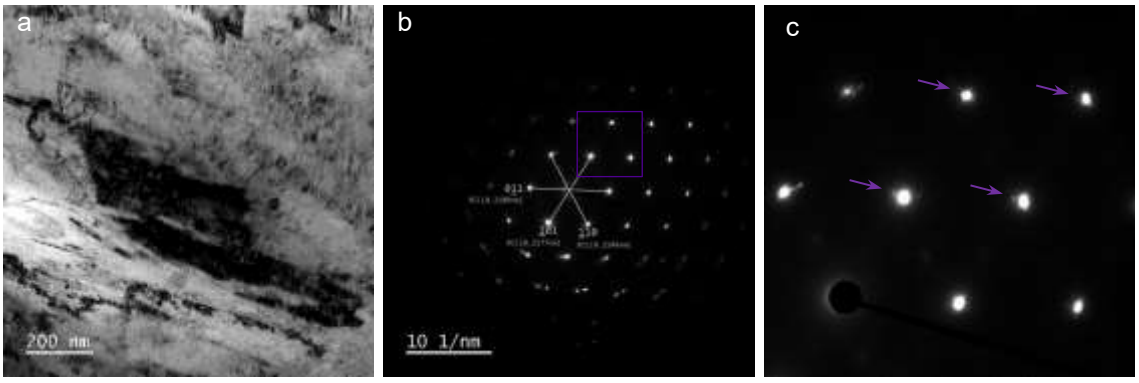

Figure 16. a) BF-TEM micrograph of an α' lath. b) SAED pattern corresponding to the mentioned lath, oriented towards $[111]$ *ZA. c) Amplification of the purple square marked in c) where spots corresponding to planes* $(10\bar{1})$, $(20\bar{2})$, $(11\bar{2})$ *and* $(21\bar{3})$ *in the direction of* $[0\bar{1}1]$

As carbon precipitation has been sequenced, before carbide formation, carbon tends to aggregate forming clustering. At a certain point, clusters that are randomly distributed

around ferrite must generate partial ordering. It has been reported satellite spots in diffraction patterns associated to this partial ordering.

4.3.2 Displacive transformation and accommodation strain

As previously discussed, the diffusionless nature of the phase transformation in both martensite and bainite requires certain degree of deformation to be accommodated. This deformation accumulates elastically in the direction of growth of the ferrite until it exceeds the tension necessary for the activation of plastic deformation: it is first accumulated in the retained austenite, and later in the ferrite.

This strain plays an important role in the mechanical properties of the steel. In non-tempered martensite the dislocation density and residual elastic strain are responsible for outstanding hardness, but also the lack of toughness.

One of the main mechanisms by which retained austenite accumulates plastic deformation is stacking faults in the form of nano-twinning. In Figure 17 we can see an austenite block located between different bainitic ferrite sheaves in a sample of B220. In both BF and DF diffraction contrast reveals twinning, we can observe parallel banding caused by the different orientations.

In the case of bainitic ferrite, transformation stresses accommodated plastically leaving trails as dislocations. Figure 18 represents a bainitic ferrite plate where dislocations have accumulated forming forests perpendicularly to the growth direction.

In the martensitic samples traces of deformation were found at M220 in the form of twins. In this case, Figure 19 shows an example of retained austenite where arrows indicate the presence of twins. It has been found similar observations in retained austenite in mechanically deformed bainitic steels [50].

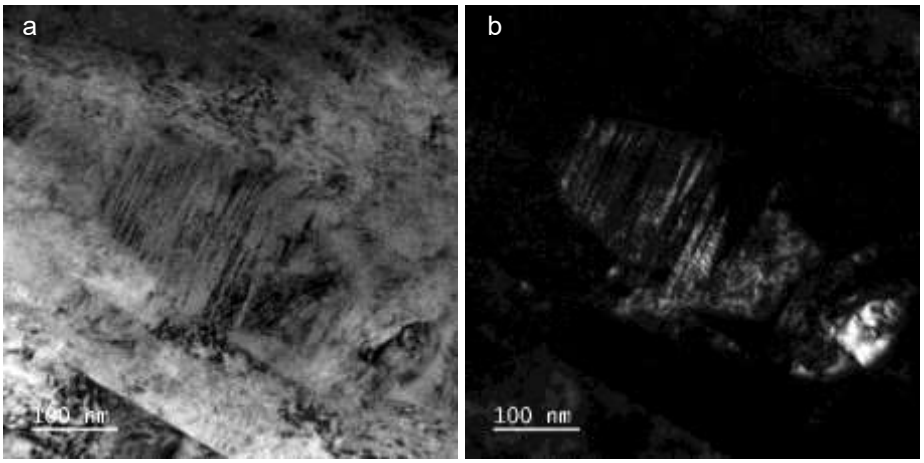

Figure 17. a) BF micrograph corresponding to an austenite block in B220, b) DF micrograph of the same area

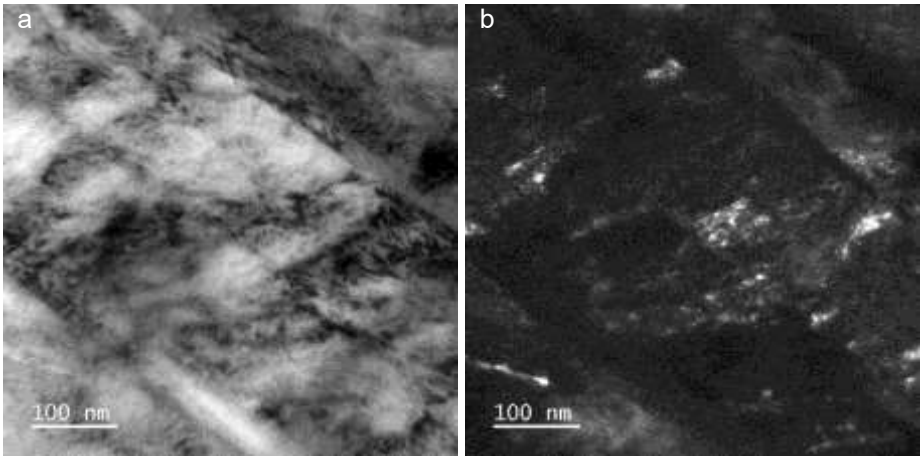

Figure 18. TEM micrograph of a B220 sample where dislocations forests are observed. a) and b) are BF and DF respectively.

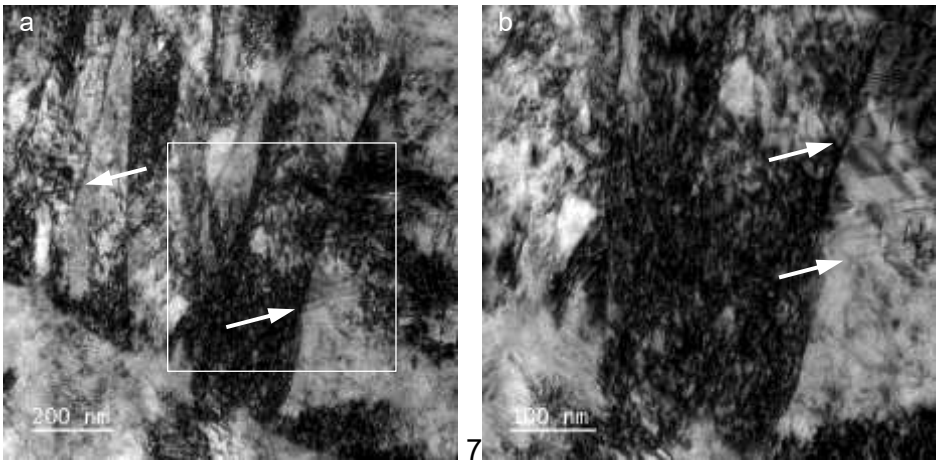

Figure 19. BF-TEM micrographs from a M220 sample where it can be found indicated by arrows dislocation steps formed on displacive transformation accommodation. b) shows a detailed view of the area marked in a white square in a).

5. CONCLUSIONS

A microstructural study of two isothermal heat treatments applied to high-silicon high-carbon steels has been carried out by transmission electron microscopy analysis. Microstructures obtained correspond to bainitic and martensitic steels.

Both iron transformations are displacive. In the case of martensite, quenching makes ferrite supersaturated and tempering permits carbon diffusion allowing partitioning and precipitating. In the case of bainite, partial quenching allows carbon to partition and precipitate during austempering.

Carbon diffusion produces the precipitation of carbides. This process occurs through a step sequence that starts by the agglomeration around dislocations, intermediate carbides, and ferrite. This sequence leaves different features in each treatment.

Bainitic ferrite contains less carbon because it could diffuse during transformation, giving precipitation in between ferrite, or stabilizing austenite. Carbon distribution inside bainitic ferrite consists more in clustering and small precipitates.

Martensitic ferrite contains higher carbon concentration due to lack of diffusion during phase transformation. Driving force for the carbide precipitation at subsequent tempering is higher than in austempering of bainitic steels and, therefore, more carbides are found inside martensitic ferrite.

Strain accommodation of the displacive transformation in bainitic ferrite consists in greater presence of dislocation (dislocation forest), whereas in martensitic ferrite fewer dislocations could be found but those had associated larger strain (dislocation steps).

6. FUTURE WORKS

The research carried out in this project was focused in the study of the microstructures found in the final product of isothermal heat treatments: tempering and austempering. The study of the material *as quenched* would have given additional understanding of the process.

The study of carbon distribution depended mainly on the comparison of the data obtained with data from previous studies. Due to the scale of the structure of these materials, the study of supersaturated and semi-saturated martensite and bainite and the control of thickness of TEM samples are crucial. Therefore, FIB techniques could be applied for thinner samples obtaining better resolutions and results. Furthermore, other techniques such as EDX or EELS would be needed to perform compositional microanalysis that could corroborate the estimations carried out in this work.

Magnetic properties of the material could have induced defects on the SAED patterns, and the images obtained. Better sample preparation and specific configuration could have improved the information obtained.

7. ACKNOWLEDGEMENTS

As the author of this manuscript, I am grateful to Tampere University for the opportunity to carry out my studies. I would like to also thank laboratories and technicians: Phase transformation (Mr. Miguel Acedo Ojeda) and X-ray diffraction (Ms. Irene Llorente) at CENIM - CSIC, and Tampere Center of Microscopy (Dr. Mari Honkanen). Special mention to Prof. Minnamari Vippola and Prof. Francisca García Caballero for the guidance and tutorship of this work.

REFERENCES

[1] J. W. Morgan and E. Anders, “Chemical composition of Earth, Venus, and Mercury.,” *Proc. Natl. Acad. Sci. U. S. A.*, vol. 77, no. 12, pp. 6973–7, Dec. 1980.

[2] D. L. Anderson, “Appendix ‘Theory of the Earth,’” *Theory of the Earth*, vol. 52, no. 1354, pp. 569–569, 1989.

[3] D. Bernhardt and J. F. Reilly, “Mineral Commodity Summaries,” 2019.

[4] R. F. Tylecote and Institute of Materials (Great Britain), *A history of metallurgy*. Maney Pub., for the Institute of Materials, 2002.

[5] “Ferrous Division WORLD STEEL RECYCLING IN FIGURES 2013-2017 Steel Scrap-a Raw Material for Steelmaking,” 2018.

[6] “Steel is the World’s Most Recycled Material | SRI - Steel Recycling Institute.” [Online]. Available: https://www.steelsustainability.org/recycling. [Accessed: 19-Nov-2019].

[7] “Circular Economy - worldsteel.” [Online]. Available: https://circulareconomy.worldsteel.org/. [Accessed: 19-Nov-2019].

[8] World Steel Association, “Steel Statistical Yearbook: 2018,” *World Steel Association*, 2017. [Online]. Available: https://www.worldsteel.org/en/dam/jcr:e5a8eda5-4b46-4892-856b-00908b5ab492/SSY_2018.pdf. [Accessed: 10-May-2019].

[9] “Periodic Table of the Elements,” in *Materials Characterization*, ASM International, 1986, pp. 688–688.

[10] W. D. Callister and D. G. Rethwisch, *Materials science and engineering*. Wiley, 2015.

[11] D. S. MacKenzie, “History of quenching,” *Int. Heat Treat. Surf. Eng.*, vol. 2, no. 2, pp. 68–73, Jun. 2008.

[12] M. F. Ashby and D. R. H. (David R. H. Jones, *Engineering materials 2 : an introduction to microstructures, processing and design*. Elsevier, 2006.

[13] W. F. Smith and J. Hashemi, *Foundations of materials science and engineering*, 4th ed. McGraw-Hill Higher Education, 2009.

[14] M. J. Donachie, *Titanium: A Technical Guide, 2nd Edition*, vol. 99, no. 5. 2000.

[15] Z. Nishiyama, *Martensitic Transformation.* Elsevier Science, 1978.

[16] B. Edgar C., “Crystal structure of solid solutions.,” *Trans. Am. Inst. Min. Metall. Eng.*, vol. 68, no. 25–46, 1923.

[17] R. Rementeria *et al.*, “Carbon Clustering in Low-Temperature Bainite,” *Metall. Mater. Trans. A*, vol. 49, no. 11, pp. 5277–5287, Nov. 2018.

[18] Z. Zhang, R. A. Farrar, and E. Institute of Materials (London, *An atlas of continuous cooling transformation (CCT) diagrams applicable to low carbon low alloy weld metals*. Institute of Materials, 1995.

[19] S. A. Sajjadi and S. M. Zebarjad, “Isothermal transformation of austenite to bainite in high carbon steels,” *J. Mater. Process. Technol.*, vol. 189, no. 1–3, pp. 107–113, Jul. 2007.

[20] American Society of Metals, *Atlas of isothermal transformation and cooling transformation diagrams*. Michigan University, 1977.

[21] H. K. D. H. Bhadeshia, “The first bulk nanostructured metal,” *Sci. Technol. Adv. Mater.*, vol. 14, no. 1, Feb. 2013.

[22] H. K. D. H. Bhadeshia, “The bainite transformation: unresolved issues,” *Mater. Sci. Eng. A*, vol. 273–275, pp. 58–66, Dec. 1999.

[23] I. Loginova, J. Ågren, and G. Amberg, “On the formation of Widmanstätten ferrite in binary Fe-C - Phase-field approach,” *Acta Mater.*, vol. 52, no. 13, pp. 4055–4063, Aug. 2004.

[24] H. K. D. H. Bhadeshia, *Bainite in steels : theory and practice*, Third edit. Cambridge.

[25] H. K. D. H. Bhadeshia, “Atomic mechanism of the bainite transformation,” *HTM - J. Heat Treat. Mater.*, vol. 72, no. 6, pp. 340–345, Dec. 2017.

[26] F. G. Caballero, M. K. Miller, C. Garcia-Mateo, and J. Cornide, “New experimental evidence of the diffusionless transformation nature of bainite,” *J. Alloys Compd.*, vol. 577, no. SUPPL. 1, Nov. 2013.

[27] F. G. Caballero, M. K. Miller, C. Garcia-Mateo, C. Capdevila, and C. Garcia de Andrés, “Phase transformation theory: A powerful tool for the design of advanced steels,” *JOM*, vol. 60, no. 12, pp. 16–21, Dec. 2008.

[28] A. Eres-Castellanos, L. Morales-Rivas, A. Latz, F. G. Caballero, and C. Garcia-Mateo, “Effect of ausforming on the anisotropy of low temperature bainitic transformation,” *Mater. Charact.*, 2018.

[29] D.-H. Huang and G. Thomas, “Metallography of Bainitic Transformation in Silicon Containing Steels.”

[30] R. Rementeria, C. Garcia-Mateo, and F. G. Caballero, “New Insights into Carbon Distribution in Bainitic Ferrite,” in *HTM Journal of Heat Treatment and Materials*, 2018, vol. 73, no. 2, pp. 68–79.

[31] B. P. J. Sandvik and H. P. Nevalainen, “Structure–property relationships in commercial low-alloy bainitic–austenitic steel with high strength, ductility, and toughness,” *Met. Technol.*, vol. 8, no. 1, pp. 213–220, Jun. 1981.

[32] J. Hu *et al.*, “Structure-mechanical property relationship in a low-C medium-Mn ultrahigh strength heavy plate steel with austenite-martensite submicro-laminate structure,” *Mater. Sci. Eng. A*, vol. 647, pp. 144–151, Oct. 2015.

[33] R. Bakhtiari and A. Ekrami, “The effect of bainite morphology on the mechanical properties of a high bainite dual phase (HBDP) steel,” *Mater. Sci. Eng. A*, vol. 525,

no. 1–2, pp. 159–165, Nov. 2009.

[34] C. García-Mateo and F. G. Caballero, “The role of retained austenite on tensile properties of steels with bainitic microstructures,” *Mater. Trans.*, vol. 46, no. 8, pp. 1839–1846, Aug. 2005.

[35] R. Rementeria *et al.*, “Quantitative assessment of carbon allocation anomalies in low temperature bainite,” *Acta Mater.*, vol. 133, pp. 333–345, Jul. 2017.

[36] C. Garcia De Andres, C. Capdevila, F. G. Caballero, and D. San Martín, “Effect of molybdenum on continuous cooling transformations in two medium carbon forging steels,” *J. Mater. Sci.*, vol. 36, no. 3, pp. 565–571, 2001.

[37] F. G. Caballero, C. García-Mateo, and C. García de Andrés, “Dilatometric Study of Reaustenitisation of High Silicon Bainitic Steels: Decomposition of Retained Austenite,” *Mater. Trans.*, vol. 46, no. 3, pp. 581–586, Mar. 2005.

[38] R. A. Young, *The Rietveld Method*, 2002nd ed. London: Oxford University Press, 1993.

[39] Dyson and D. J., “Effect of Alloying Additions on the Lattice Parameter of Austenite,” *J. Iron Steel Inst.*, vol. 208, pp. 469–474, 1970.

[40] C. Garcia-Mateo, F. G. Caballero, M. K. Miller, and J. A. Jimenez, “On measurement of carbon content in retained austenite in a nanostructured bainitic steel,” *J. Mater. Sci.*, vol. 47, no. 2, pp. 1004–1010, Jan. 2012.

[41] J. H. Jang, H. K. D. H. Bhadeshia, and D. W. Suh, “Solubility of carbon in tetragonal ferrite in equilibrium with austenite,” *Scr. Mater.*, vol. 68, no. 3–4, pp. 195–198, Feb. 2013.

[42] D. De-Castro *et al.*, “Examining the multi-scale complexity and the crystallographic hierarchy of isothermally treated bainitic and martensitic structures,” *Mater. Charact.*, vol. 160, p. 110127, Feb. 2020.

[43] R. Rementeria, “Carbon distribution in low temperature bainite,” Universidad Internacional Menéndez Pelayo (UIMP), Madrid, Spain.

[44] R. R. Rementeria *et al.*, “Carbon concentration measurements by atom probe tomography in the ferritic phase of high-silicon steels,” *Acta Mater.*, vol. 125, pp. 359–368, Feb. 2017.

[45] “X-Ray Spectrometry,” in *Materials Characterization*, ASM International, 1986, pp. 82–101.

[46] “Analytical Transmission Electron Microscopy,” in *Materials Characterization*, ASM International, 1986, pp. 429–489.

[47] M. J. Santofimia, F. G. Caballero, C. Capdevila, C. García-Mateo, and C. G. de Andrés, “Evaluation of Displacive Models for Bainite Transformation Kinetics in Steels,” *Mater. Trans.*, vol. 47, no. 6, pp. 1492–1500, Jun. 2006.

[48] G. Ghosh and G. B. Olson, “Computational thermodynamics and the kinetics of martensitic transformation,” *J. Phase Equilibria*, vol. 22, no. 3, pp. 199–207, Jun. 2001.

[49] R. Naraghi, M. Selleby, and J. Ågren, “Thermodynamics of stable and metastable structures in Fe-C system,” *Calphad Comput. Coupling Phase Diagrams Thermochem.*, vol. 46, pp. 148–158, Sep. 2014.

[50] Caballero *et al.*, “Understanding Mechanical Properties of Nano-Grained Bainitic Steels from Multiscale Structural Analysis,” *Metals (Basel).*, vol. 9, no. 4, p. 426, Apr. 2019.

This work has been produced using Microsoft Office Word 2016 and Microsoft Office 365 Word, licence granted by Universidad Politécnica de Madrid (UPM). Template for master’s thesis used was granted by Tampere Universities (TAU) and optimized.

The references of this thesis document have been managed using Mendeley Desktop software (Elsevier) and its Microsoft Office Word extension.

Access to papers, journals, books, and other bibliography was granted by Red de Bibliotecas y Archivos del CSIC, Universidad Politécnica de Madrid (UPM) and Tampere Universities (TAU).